

Numerical modeling of reaction-induced cavities in a porous rock

Anne Ormond

Observatoire Midi Pyrenées, Université P. Sabatier, Toulouse, France

Peter Ortoleva

Laboratory for Computational Geodynamics, Department of Chemistry, Indiana University, Bloomington

Abstract. The interaction between mineral reaction and mass transport in a rock can lead to reaction front instability and the development of channel-like voids. This phenomenon is studied with a two-dimensional model accounting for the nonlinear feedback between flow, reaction, and matrix porosity-permeability evolution. In our model we calculate the flow field in both the porous medium and the reaction-induced voids, using the Brinkman equation. While a linear analysis cannot determine the length scale of the channels which can develop in a typical geological system, our simulations indicate that the channel size is actually unique and well characterized. While the onset of instability is favored at a preexisting heterogeneity, the channel growth and orientation is governed by the global flow pattern, even in an initially heterogeneous system.

1. Introduction

Permeability and flow are closely related by a nonlinear feedback, through the dissolution and precipitation of minerals, in sedimentary basins or metamorphic system, on a large range of spatial scales. At regional scale the development of karst in carbonate rocks is the result of massive dissolution by subsurface fluid flow [e.g., *White*, 1988]. At the scale of a platform reef the very heterogeneous texture of the carbonate matrix is due to both the coral formation and to coupled reaction and flow within the reef [*Schreoder and Purser*, 1986; *Rougerie et al.*, 1991]. At the centimeter scale, experiments on matrix acidizing for the study of well stimulation illustrate the positive feedback between flow and reaction leading to the infiltration instability and eventually to the formation of long narrow holes referred to as “wormholes” [*Williams et al.*, 1979]. In these three examples, the flow coupled with the transport of solutes generated by mineral dissolution leads to self-organized enhancement heterogeneity in the rock. In particular, in these cases the reaction-flow feedback led to cavity formation, and hence these phenomena cannot be described via Darcy’s law everywhere within the medium. Our study is based on a numerical simulation of this phenomenon using Brinkman, not Darcy, flow. We show that observed channels can constitute a self-organized network built by the fluid flow-reaction feedback.

It is now well known that fluid flow through a soluble porous medium may result in the formation of a channel-like altered area along an advancing reaction front [*Chadam et al.* [1986]; *Ortoleva et al.* [1987]; *Hoefner and Fogler* [1988]; *Rege and Fogler* [1989]; see *Ortoleva* [1994] for a review ;

Aharonov et al. [1995] ; *Bolton et al* [1997], *Renard et al.* [1998]). Here we define fingers, channels wherein the dissolution is not total within a channel, for example, the case wherein only one mineral dissolves and some matrix still remains as an altered porous medium. We define a cavity as a void created when the channel interior matrix is completely removed through dissolution. The mechanism for this flow-reaction instability phenomenon is the following: When undersaturated fluid flows through the matrix, a region with slightly larger porosity attracts a greater flow-through. Thus locally, the rate of dissolution and, consequently, porosity and permeability increase in a positive feedback loop. The dispersion of the fluid through the tortuous porous medium tends to spread the reactive fluid and thus represses the channeling instability.

The characteristic length of the channeling is commonly related to two nondimensional numbers, that of Damköhler, $Da = G L / \bar{V}$, and that of Peclet $Pe = \bar{V} \times L / D$, which involve the reaction rate G , average fluid velocity \bar{V} , molecular dispersion coefficient D , and a length L corresponding to the width of the simulation domain or, in a natural system, to the width of the zone which is drained by the fluid. Let L_r be the reaction front thickness. It corresponds to the thickness of the zone wherein the fluid and the matrix are out of chemical equilibrium. This thickness is larger for slow reaction or large fluid velocity. Note that Da is proportional to the L/L_r ratio. For Da below 10^2 (corresponding to a system wherein $L_r \gg L$) the reaction front remains planar. For Da larger than 1 the reaction front tends to destabilize [*Steefel and Lasaga*, 1990]. For these large Da , the width of the channel-shape dissolved zone is necessarily between a few times L_r and L . The length of an elongate channel depends on the balance between advection and dispersion: When dispersion equilibrates concentration inside the channel before the fluid reaches the channel tip, growth stops. The Pe number is a measure of the balance between the two processes. *Ortoleva et al.* [1987] have shown analytically

Copyright 2000 by the American Geophysical Union.

Paper number 2000JB900116.
0148-0227/00/2000JB900116\$09.00

that for infinite Pe the channel should be infinitely long. The determination of the channel length can only be done via a resolution of the complete nonlinear problem [Chadam *et al.*, 1988]. Initial heterogeneity in the porous medium is an additional parameter that affects the characteristic of the channel structure.

A systematic study of the channeling problem has not yet been done. At the pore scale, Daccord [1987] did a spectacular experiment on plaster that shows the development of a highly branched wormhole network. It seems that the wormholes develop a complex network that can be described by a diffusion limited aggregation model. Hoefner and Fogler [1988] carried out numerical simulations that were in qualitative agreement with acidizing experiments for a large range of Da . The instability has also been studied using numerical simulation at the pore scale, where the fluid motion was described by Stokes equation (see Adler [1992] for a detailed review). Concerning the matrix heterogeneity, the transport/dissolution feedback enhances the porosity in the direction of the macroscopic flow [Bernabe, 1996]. At the suprapore (or Darcy) scale an additional scale of heterogeneity can interact with the progress of the reaction front.

Fingering has been modeled using the Darcy equation, which can be applied in both homogeneous and heterogeneous porous media, as long as the dissolution process does not increase the porosity dramatically. Chen and Ortoleva [1990] modeled many examples of fingers that develop and split into branches. It has been shown that an increase of the fluid advection rate (increase of Pe) leads to narrower and longer fingers [Steefel and Lasaga, 1990; Chen and Ortoleva, 1990]. It has not been established whether the width and density of developing channels is determined by the characteristic of the system; however, numerical simulation appears to be a promising way to study this phenomenon.

Numerical simulation of wormholes has been achieved using Brinkman's equation. This equation describes fluid transport both in porous medium and voids [Liu *et al.*, 1997]. In this study we use our two-dimensional (2-D) Darcy-scale Brinkman numerical simulator to characterize the size and number of channels which grow in (1) a homogeneous medium where only one of two minerals dissolves (yielding fingers), (2) a homogeneous medium with one mineral (yielding cavities), and (3) a medium with heterogeneous initial permeability. We show that the size of channels is determined by the system's fluid/rock chemical and hydrodynamic characteristics. Additionally, we show that the interplay of initial heterogeneity with self-organizing infiltration prevents complex channel splitting in a naturally heterogeneous medium. Since geological systems wherein channeling may occur display a large range of spatial scales, we decided to do the simulation at the experimental scale in a way that our results may be compared to existing or future experimental data.

2. Model Formulation

Our model is based on conservation of mass and momentum equations. The equations are coupled through the dependence of permeability on matrix properties. They are solved using finite difference and iterative techniques.

2.1. Matrix Description and Permeability Law

The matrix is constituted of spherical grains, each consisting of a single mineral, with specified radius and number per volume. For a homogeneous medium these variables are initially the same everywhere. For a heterogeneous medium the radius $R_i(x, y)$ of minerals is chosen to be a random distribution. The porosity ϕ (volume fraction of the rock occupied by fluid) satisfies

$$\phi + \sum_{i=1}^N n_i V_i = 1, \quad (1)$$

$$V_i = \frac{4}{3} \pi R_i^3, \quad (2)$$

where N is the number of minerals and n_i and V_i are the number per rock volume and the volume of mineral i spherical grains, respectively. A summary of the notation we use can be found in Table 1. The permeability κ is a function of the porosity and grain radii. The Fair-Hatch empirical equation [Bear, 1972, p. 134] is used for porosity smaller than 50%, in the modified form

$$k = \frac{\phi^3}{J(1-\phi)^2} \times \frac{1}{\left[\sum_{i=1}^N \theta n_i V_i / R_i \right]^2}. \quad (3)$$

Here J ($= 5$) is a grain-packing factor and θ is a geometric factor (assumed to be 6 for spherical grains). For porosity larger than 50%, the Fair-Hatch equation is not valid. There are no experimental data to formulate a permeability law for large porosity. We choose to increase the permeability via an ad hoc function of porosity in the form $\kappa = 10^{-15}/(1-\phi)^{11}$ so that κ is, 10^{-12} m^2 (1 darcy), 10^{-10} m^2 , and 10^{-2} m^2 for porosities of 50, 70 and 90%, respectively.

2.2. Chemical Model

The thermodynamic data for the mineral and aqueous reactions are taken from the EQ3NR data bank [Wolery, 1992], at room temperature and pressure. Since the kinetics of the quartz reaction typically more than 6 orders of magnitude slower than that of calcite, in our study, quartz is not involved in the dissolution-precipitation process.

The calcite reaction is assumed to proceed via



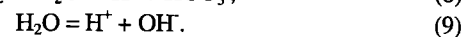
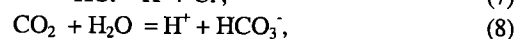
The rate of dissolution of mineral i grains, denoted G_i (in m s^{-1}) is taken in the form

$$G_i = \frac{k_i}{K_i} \left(K_i \prod_{v_\alpha < 0} a_\alpha^{v_\alpha} - \prod_{v_\alpha > 0} a_\alpha^{v_\alpha} \right), \quad (5)$$

with a_α the activity of aqueous species α and v_α the stoichiometric coefficient for species α in the mineral i reaction. K_i is the equilibrium constant for the mineral i reaction at room temperature and pressure, and k_i (in m s^{-1}) is the rate constant of the mineral i reaction. The feedback between matrix evolution and reaction is accounted for with the grain growth rate:

$$\frac{\partial R_i}{\partial t} = G_i. \quad (6)$$

The following aqueous reactions are assumed to be fast and hence maintained near equilibrium :



The system is assumed to support only one fluid phase (no out-gazing is considered). The equations of the conservation of the aqueous species α take the form

$$\frac{\partial \phi C_{\alpha}}{\partial t} = -\nabla \cdot (-D \nabla C_{\alpha} + \phi \mathbf{V} C_{\alpha}) + \sum_{j=1}^{N^f} v_{\alpha}^j W^j + \sum_{j=1}^{N^s} v_{\alpha}^j W^j, \quad (10)$$

$$W^i = 4\pi R_i^2 G_i. \quad (11)$$

Here W^i is the reaction rate for the aqueous reaction and N^f is the number of fast aqueous reaction. The ρ_i is the molar density of mineral i , and D is the dispersion coefficient for species in the aqueous fluid, is taken to be the same for all species, and is proportional to the magnitude of the flow velocity. The analysis of the conservation equations (10), in the limit of fast aqueous reaction, is given in chapter 3 of *Ortoleva [1994]*.

2.3. Fluid Mass and Momentum Balance

The Darcy velocity $\phi \mathbf{V}$ is an average of the fluid velocity over the volume of the rock including solid and pore volumes. If the flow is laminar and the porosity is low, Darcy's law takes the form

$$\frac{\mu}{\kappa} \phi \mathbf{V} = -\nabla P. \quad (12)$$

Here μ (in Pa s) is the fluid viscosity, κ is the permeability, and P is the fluid pressure. If the medium contains secondary features such as a cavity that is much larger than the volume over which Darcy velocity is calculated through averaging, this equation does not apply within the cavity because the permeability diverges there. In the voids the flow has to be calculated with Stokes' equation. This raises the problem of the continuity of variables (velocity and pressure) between the porous medium and the cavity. To describe such phenomena, *Brinkman [1947]* integrated Stokes' and Darcy's laws in the flow law

$$\frac{\mu}{\kappa} \phi \mathbf{V} - \mu \nabla^2 \phi \mathbf{V} = -\nabla P. \quad (13)$$

Numerical solution of Brinkman's equation shows that where permeability is smaller than 10^{-10} m^2 (100 darcies), the Laplacian term, is negligible compared to the linear velocity term and the equation is reduced to Darcy's law. Where permeability is larger than 10^{-4} m^2 , (13) yields Stokes' flow. Experimental and numerical studies [*Arquis, 1994, 1995*] show that the Brinkman equation adequately captures the velocity of the fluid in the boundary layer between the porous medium and the free fluid zone as well.

During a time step the volume of fluid drained by the advective flow is 3 orders of magnitude larger than the increase of fluid volume due to the increase of porosity. Consequently the system fulfills the quasi-stationary approximation [*Lichtner, 1988*], and mass conservation resumes:

$$\nabla \cdot (\phi \mathbf{V}) = 0, \quad (14)$$

the incompressibility condition.

2.4. Numerical Simulation Approach

We numerically solve the equations for the conservation of mass for the aqueous species using a finite difference technique [*Liu et al., 1997*]. The Brinkman equation was

solved using finite difference discretization and a penalty technique [*Peyret and Taylor, 1982*]. The principle of the method is based on the introduction of artificial compressibility and time dependence to the momentum (13) and mass (14) conservation equations such that

$$\frac{\partial \phi \mathbf{V}}{\partial t} + \frac{\mu}{\kappa} \phi \mathbf{V} - \mu \nabla^2 \phi \mathbf{V} = -\nabla P, \quad (15)$$

$$\frac{\partial P}{\partial t} = -\frac{\nabla \cdot (\phi \mathbf{V})}{\chi}. \quad (16)$$

Here t and χ correspond to an artificial time and compressibility. Equations (15) and (16) are solved in an iterative process until a steady state solution is reached. The values of the time step and χ are adjusted to speed convergence.

The physical time step for evolution through all the conservation equations is chosen so that a maximum change of 1% of the grain radius by dissolution is attained. Consequently, this time step controls the change of velocity of the fluid and the advancement of the reactions.

2.5. Initial and Boundary Conditions

The domain is initially saturated with water at chemical equilibrium with all minerals. Upper and lower boundaries of the 2-D domain are assumed impermeable: normal velocity and normal derivative of the shear velocity are taken to be zero, which is compatible with the momentum and mass conservation equations. A difference of pressure between the inlet (left) and outlet (right) boundaries induces the overall flow. The shear velocity and the shear partial derivative of the normal velocity are taken to be zero, on both inlet and outlet boundaries.

2.6. Nondimensional Equations and Parameters

A nondimensional form of the conservation equations (10), (13) and (14) clarifies the role of Pe and Da . We use the conventional scaling factors (noted with an asterisk) introduced by *Békri et al. [1995]*:

$$\nabla^* = L \nabla, \quad x^* = \frac{x}{L}, \quad \mathbf{V}^* = \frac{\mathbf{V}}{\bar{V}}, \quad P^* = \frac{PL}{\mu \bar{V}},$$

$$t^* = \frac{tD}{L^2}, \quad c_{\alpha}^* = \frac{c_{\max} - C_{\alpha}}{c_{\max} - c}, \quad \kappa^* = \frac{\kappa}{\kappa_0}, \quad (17)$$

with L , \bar{V} , and D the characteristic length, average interstitial velocity and dispersion taken in Pe and Da evaluation. With c_{\max} and \bar{c} the maximum and average concentration of the aqueous species. The system becomes :

$$\nabla^* \cdot (\phi \mathbf{V}^*) = 0 \quad (18)$$

$$\phi \mathbf{V}^* - \kappa^* \nabla^{*2} \phi \mathbf{V}^* = -\nabla^* P^* \quad (19)$$

$$\frac{\partial \phi C_{\alpha}}{\partial t^*} = \nabla^{*2} c_{\alpha}^* - Pe \nabla^* (\phi \mathbf{V}^* c_{\alpha}^*) + Pe \cdot Da \mathfrak{R}(c_{\alpha}^*). \quad (20)$$

The last term in (20) is a source term for species α resulting from the mineral and aqueous reactions of (10). In the simpler case of a one-mineral reaction with a first-order rate this term is c_{α}^* times $Pe Da$. In that form the dissolution rate is clearly enhanced by large Pe and Da .

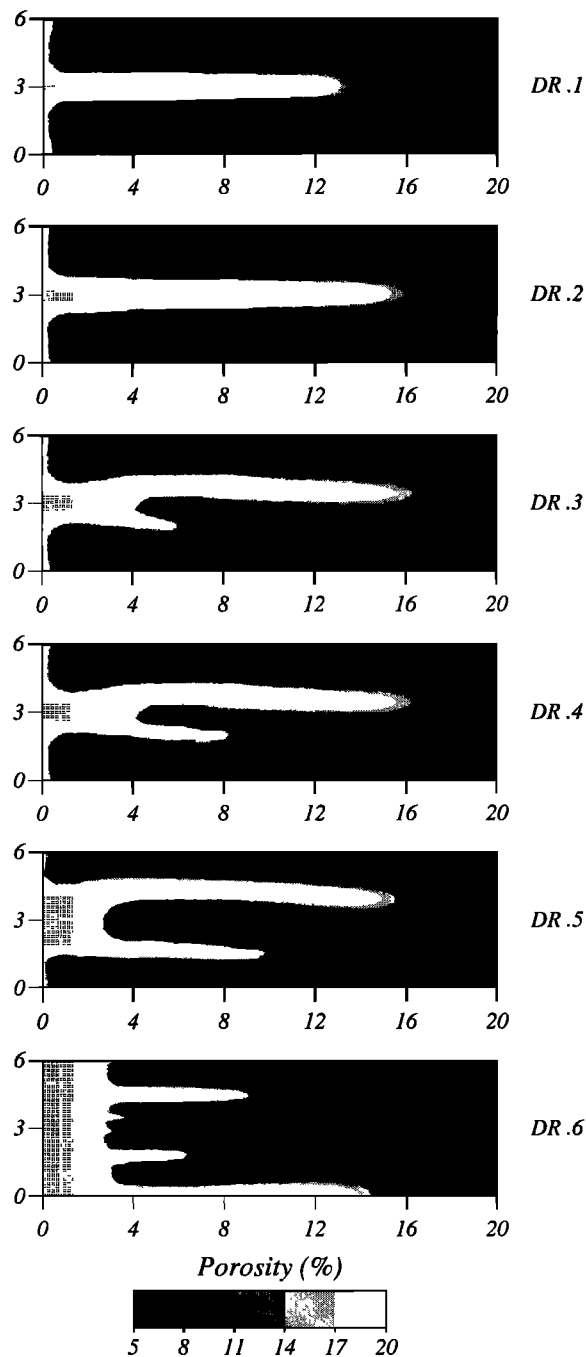


Figure 1. Final porosity after ≈ 2400 s, for all finger simulations including an initial matrix with 80% quartz and 15% calcite. The finger is the result of the dissolution of calcite. The size of the domain is expressed everywhere in 10^{-2} m. The dotted area represents the initial hole without calcite in the matrix. Its size is 1.4×10^{-2} m by 0.18×10^{-2} m (DR.1), 0.47×10^{-2} m (DR.2), 0.59×10^{-2} m (DR.3), 0.71×10^{-2} m (DR.4), and 2.14×10^{-2} m (DR.5). For DR.6 the dotted area does not represent a hole, but the area where the initial volume of calcite is perturbed by a white noise.

3. Numerical Simulations

3.1. Validation

The resolution of the chemical equations coupled with Darcy's equation has been used for previous studies including the fingering in carbonate-cemented sandstone [Chen and

Ortoleva, 1990] and deep well waste injection [Ortoleva *et al.*, 1996]. The evolution of the concentration of aqueous species has been fitted to experiments on rock samples [Liu *et al.*, 1997]. The solution of Brinkman's equation has been used by us earlier for the simulation of wormholing in carbonate system [Liu *et al.*, 1997]; these results concerning size, shape, and growth rate of the wormholes were comparable to experimental results (B. Bazin, personal communication, 1998).

3.2. Parameters for the Simulations

The characteristics of the reactive fluid and the size of the porous domain were chosen to get a system with large Pe and Da , as is typical of a geological system. Parameters include an effective reaction rate of 10^{-3} m s^{-1} . The initial average fluid velocity is 10^{-5} m s^{-1} but increases to 10^{-4} m s^{-1} during the simulation because of the constant pressure boundary conditions of the simulations. The dispersion is proportional to the velocity and the grain radius and is in the range $10^{-9} - 10^{-8} \text{ m}^2 \text{ s}^{-1}$. The order of magnitude of the characteristic length scale L (width of the simulation domain in the vertical direction) is 10^{-1} m. With these parameters we get during the simulation a reaction front thickness such that L is at least 20 times larger than L_r . This system allows the formation of several channels. It is important to note that a good numerical resolution requires at least a few grid points in the reaction front. Our 200 by 200 grid allows us to simulate up to 10 adjacent channels without compromising the quality of our solutions. The length of the domain is 2 times L . These parameters bring Da to above 1 and Pe to above 10^2 . As a consequence, any heterogeneity can trigger an instability of the planar reaction front. The porous medium is taken to be characteristic of a sedimentary rock with initial porosity of 5%, corresponding to a permeability of 10^{-15} m^2 (10^{-3} darcies). The concentration of aqueous species in the inlet fluid is 0.1 mol kg^{-1} for H^+ and Cl^- , $10^{-4} \text{ mol kg}^{-1}$ for Ca^{++} , HCO_3^- , $\text{CO}_2(\text{aq})$, and SiO_2 , and 1 mol kg^{-1} for H_2O .

The cases that we present fall into three general series. The first is referred to as DR, from Darcy resolution; it yields fingering as these systems contain a background insoluble quartz matrix. The series of BR (from Brinkman resolution) yields cavities. The H series is used to analyze the effect of the initial heterogeneity on the development of cavities.

3.3. Darcy Regime: Reaction Front Fingering

The porous medium initially contained 15% calcite and 80% quartz. Fingering develops through the dissolution of calcite. We ran the same simulation except for different widths of an initial heterogeneity that took the form of a rectangle without calcite at the inlet of length 1.4×10^{-2} m and widths 0.18×10^{-2} , 0.47×10^{-2} , 0.59×10^{-2} , 0.71×10^{-2} and 2.14×10^{-2} m (corresponding to a size between 0.5 and $4 L_r$). The time for a finger to reach the outlet side of the domain was 10 - 20 hours, depending on how many fingers develop. We analyze the resulting pattern after dissolution of the calcite but just before breakthrough at the outlet, regardless of the number and shape of the fingers which developed.

The first result of these simulations (Figure 1) is that either one or two fingers develop, depending on the width of the initial heterogeneity. When it is narrower than 0.59×10^{-2} m (roughly, $2 L_r$), only one finger develops (cases DR.1, and DR.2). In these cases the finger widens to

1.34×10^{-2} m by the time it reaches the outlet (at ≈ 10 hours). The size and growth rate (m s^{-1}) of the fingers are independent of the width of the initial heterogeneity in this range of initial width. However, when the initial heterogeneity is wider than 0.59×10^{-2} m (cases DR.3, DR.4, and DR.5) two fingers develop starting from each downstream corner of the initial heterogeneity; in these cases one of the fingers stops growing while the remaining finger grows wider and evolves toward the center of the domain, eventually reaching the outlet. The wider the initial heterogeneity, the longer both fingers survive. This set of simulations suggests that two fingers cannot develop too close to one another. *Hoefner and Fogler* [1988] proposed that two fingers could not grow longer than the distance between them. Though in our simulation the length of the two surviving fingers grows longer than the separating distance, there is a qualitative agreement in the fact that the length of the fingers is proportional to the distance between them. This series illustrates the competition between fingers in a system where the dissolution is limited by advection. The bending of the remaining finger toward the middle of the domain along the largest pressure gradient line, which is controlled by the boundaries, illustrates that the largest pressure gradient (which induces the highest local fluid velocity) is closely related to the shape of the finger. The second result is that regardless of the initial heterogeneity, we get the same finger width (a few L_r). From the widest heterogeneity no wide finger develops; the system rather supports two narrower fingers, even if one is to be abandoned by the flow early.

In case DR.6 the homogeneous matrix was perturbed with an initial white noise, in a 1.4×10^{-2} m wide strip so that every length scale which can perturb the reaction front is excited. At the beginning several small fingers develop. Each of the fingers grew at the same rate and thus had the same length and, consequently, the same amount of fluid. Essentially, all the fluid was drained by the fingers and not by the matrix between them. Once the fingers reach a size such that they compete for the fluid, those which are closer to each other grow slower. Once a finger is slightly shorter than the neighbors, it ceases growth. Fingers stopped growing in areas where their initial number was the highest. The final pattern of dissolution provides a record of the evolution of the flow. It is a pure hydrodynamics phenomenon resulting from the competition for fluid capture among neighboring fingers. This set of simulations (characterized by L , G , \bar{V} , and D) shows that this system leads to the final growth of one stable finger. The width of the finger is independent of the size of the initial heterogeneity, at the inlet side. It is ≈ 4 times the thickness of the reaction front when it reaches the outlet. No very large finger develops either from a larger initial heterogeneity or from the white noise heterogeneity. In this sense, fingering is robust.

From this result we expect that in an infinitely wide domain (large L , Pe , and Da) the width of the developing finger will be the same as the size that we found in the simulations of Figure 1. The number of actively growing fingers will decrease with time because the longer the finger, the wider the area that it dominates. The distance between surviving fingers and the maximum length reached by a growing finger can only be found by the simulation of a large domain, for large times. We do not attempt to obtain large-time, finger-spacing, and length-scaling laws here, although we believe they do exist.

The simulation of a domain with infinite L cannot be done by wraparound boundary conditions because in both periodic and no-flow boundaries at top and bottom (in the present study), constraints on the amount of drainage are imposed to be L times V . It is, however, significant to double the domain width L over that of the previous system (which doubles Pe and Da as well). In Figure 2 we started the simulation in a domain where the initial heterogeneity is generated by the same white noise as used for the narrow domain in the lower half of the wider domain. In this double-width domain the long-time consequence is again a single dominant finger. This demonstrates a type of scaling whereby the time to obtain a single dominant finger increases with the width of the system (although we did not determine the scaling exponent). We find that the finger growth rate and size are similar as long as more than one finger grows (during the first 800 s). What could not be predicted is whether one or two fingers would eventually reach the outlet of the domain, in the 2 times wider domain. Because of the initial white noise condition one finger happened to grow in a more isolated area (and got more fluid) in the wider domain than in the narrower one. This finger became dominant in the top part of the wider domain before one of the two fingers became dominant in the narrow domain. Since again in the wider domain only one finger reached the outlet, the only prediction which can be made is that in an infinitely wide domain the distance separating two fingers, longer than the domain length (in Figure 2), will be at least larger than $L = 0.12$ m.

3.4. Brinkman Versus Darcy Flow: Creation of Cavities

To compare the development of fingers in a porous medium with that of empty cavities, we run the experiments with the same set of parameters as in the DR series, except that the solid phase is now only calcite. We present two simulations, BR.1 and BR.2 (Figure 3), with initial heterogeneity areas 0.18×10^{-2} m ($< L_r$), and 0.71×10^{-2} m ($> L_r$) respectively. The initial high-porosity area in the matrix near the inlet corresponds, to DR.1 and DR.3, respectively. In the BR series, whether the initial heterogeneity develops into one cavity or splits into two cavities is independent of its initial width, for the parameters used here. In case BR.1 the two cavities grow with the same width (0.52×10^{-2} m), but unlike in the DR cases, when only one cavity remains, it grows without getting wider. A similar trend is observed in BR.2; both cavities show the same width (0.59×10^{-2} m). In both BR cases (and another we do not present here) the cavities that develop are $\approx 30\%$ narrower than the fingers.

To see the specific effect of the fluid motion on the development of the instability, we compare the flow pattern and porosity in a cross section through a finger and a cavity in a case where only one straight channel develops (Figure 4). The initial porosity is 7% in both cases, with 93 and 35% of calcite for BR and DR, respectively. At the end of the simulations the increase of porosity through a cross section is very similar in both cases: Porosity is constant in the unaltered zone, and the transition to the channel is marked by a sharp stepwise increase in porosity. It occurs in a zone thinner than 0.5×10^{-2} m, which represents locally the upper limit of L_r . This is in agreement with a large Da inducing a small L_r compared to L , in both cases.

In Figure 4 we show that the altered zone is $\approx 30\%$ narrower in the BR case than in the DR case. In the BR case the velocity profile is parabolic, while in the DR case it is flat

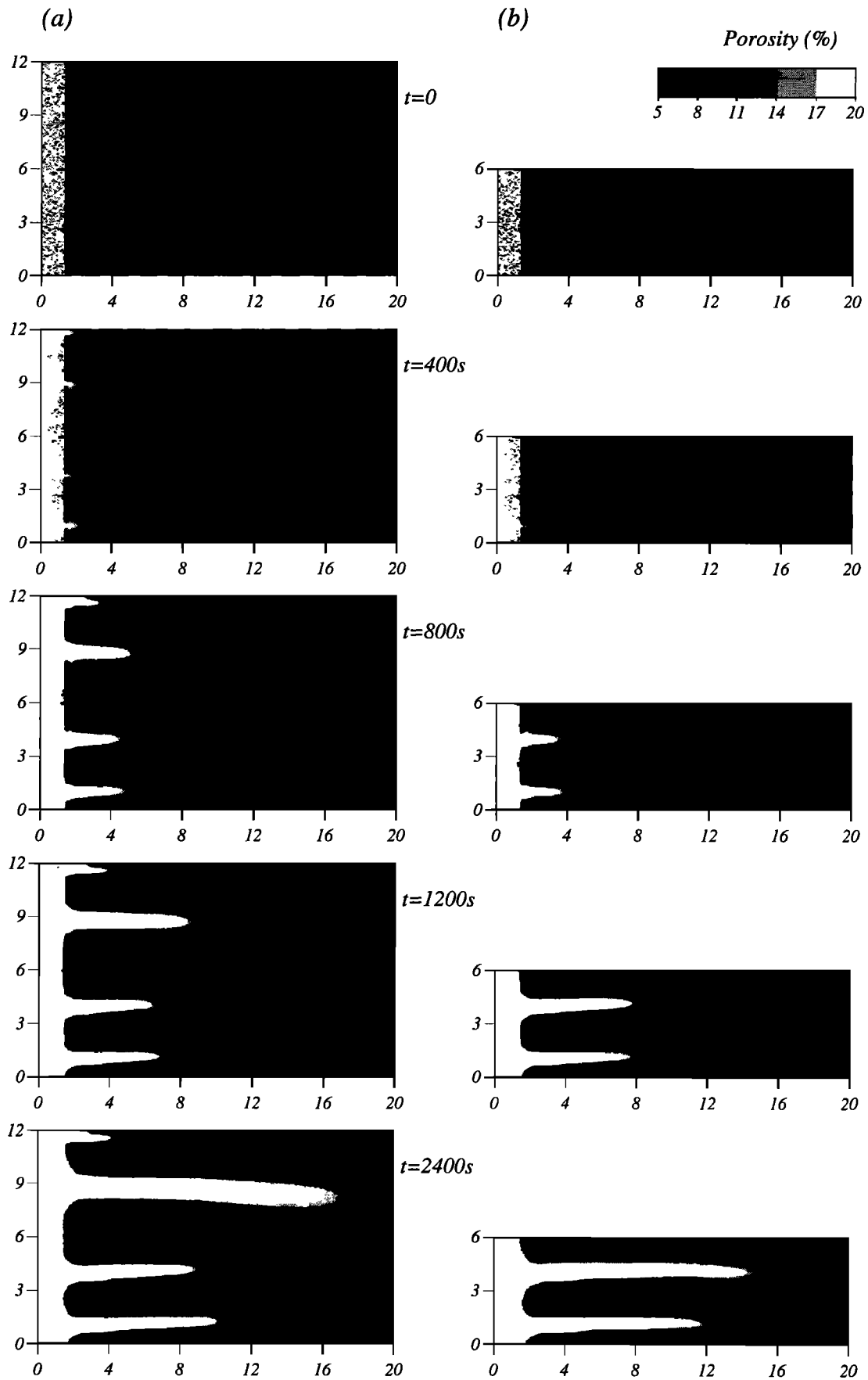


Figure 2. Time evolution of porosity for finger simulations in a matrix with 80% quartz and 15% calcite. Fingers are the result of dissolution of calcite. Box size is 20×10^{-2} m by (a) 6×10^{-2} m and (b) 12×10^{-2} m. The initial heterogeneity in permeability (domain wide strip) is the same in Figure 2a as in the lower half of Figure 2b.

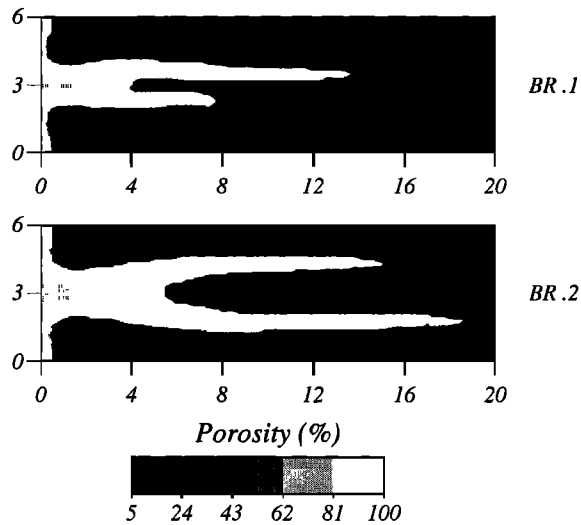


Figure 3. Porosity field after ≈ 60 hours for the simulations of cavities, in a calcite matrix which initially had 5% porosity. The dotted area represents 100% of porosity in the initial matrix. Its size is 1.4×10^{-2} m by 0.18×10^{-2} m (BR.1) and 0.71×10^{-2} m (BR.2).

within most of the finger. In the BR case we find laminar flow of Poiseuille in a channel, while in the DR case the velocity inside the finger is proportional to the permeability. The maximum filtration velocity is the same in both cases since it is controlled by the maximum pressure gradient and by the permeability between the tip of the finger and the outlet side of the domain. As a consequence, the fluid velocity in the pore volume is higher in the DR cases where porosity is lower. Since dispersion is proportional to fluid velocity, it is larger in a larger area along the side of the finger for DR cases. This larger dispersion prevents the formation of a chemical boundary layer along the side of the finger. In the BR case the flow pattern is such that there is a no-slip flow boundary condition at the interface between the cavity and the nonaltered porous medium. A consequence is that more reactive fluid reaches the tip of the channel. This may allow the development of longer and narrower cavities. Eventually, since fluid velocity is slower, the global flow across a vertical section (parallel to the channel development direction) brings slightly less reactive fluid to dissolve the calcite, per unit time. Additionally, the channel growth is much slower in the BR cases because the amount of calcite to dissolve is 40% larger. All these differences between the growth of fingers and cavities are summarized in Table 1.

3.5. Cavity Growth in Heterogeneous Media

In the following simulations the porous medium is heterogeneous in the whole domain. At each grid point (corresponding to a referenced elementary volume) the radius of the spherical grains is chosen from a uniform random distribution between the values of 5×10^{-8} and 10^{-5} m. For every simulation in this section, we use the same series of random numbers; as a consequence, the medium contains the same pattern of initial heterogeneity. As in the homogeneous cases, the initial porosity is kept at 5% everywhere. Since the permeability of the medium is expressed as a function of porosity and grain radius, the initial permeability is correlated with the variation in the initial grain size (Figure 5a).

Heterogeneity focuses fluid where the permeability is large. As a result, for the same pressure gradient, and averaged permeability, the maximum fluid velocity is larger in the heterogeneous medium than in the homogeneous one. Since fluid focusing induces reaction front instability, we expect that heterogeneity will not only induce but also foster the development of cavities. As for the homogeneous cases, we carry out two kinds of simulations: (1) We favor the development of a channel characterized by the width of the non-uniformity that we add in the initial matrix (that therefore favors the potential development of a wavelength), and (2) all the wavelengths are excited at the inlet by a white noise in the heterogeneous distribution of the initial matrix.

First we made a series of three simulations with an additional initial disturbance near the inlet side. The length of the zone is 1.42×10^{-2} m while its width is first set to 0.18×10^{-2} m (as in DR.1 and BR.1), in a second case, to 0.71×10^{-2} m (as in DR.3 and BR.2), and, then, to 1.42×10^{-2} m (as in DR.5). Each case ultimately resulted in the development of only one cavity with the same final shape and width. Similarly, as for DR and BR, the progress and destabilization of the reaction front does not depend on the size of the initial inlet heterogeneity.

Case H.1 (Figure 5b) shows the growth of the channel starting from the 0.18×10^{-2} m wide rectangular heterogeneity. The resulting cavity looks very similar to BR.1. The width of the cavity in H.1 is the same as that of the longest cavity in BR.1. As expected, the reaction front is not as smooth as in the homogeneous cases. The roughness length scale is equivalent to the reaction front thickness. During simulation BR.1 the cavity splits when it is 3×10^{-2} m long. In H.1 too, there is evidence of splitting at 3×10^{-2} m from the inlet, where the cavity is swollen. Indeed, during the simulation the splitting aborts soon after it starts. It takes 162×10^3 s (45 hours) to get to the point of splitting for the case BR.1, but only 113.8×10^3 s (31.6 hours) for H.1. After the aborted splitting, the single cavity of H.1 grows much faster than the double-channel pattern of BR.1 because, as we have already noted in section 3.3., one cavity grows faster than do two cavities simultaneously. The faster growth rate of the cavity in case H.1 (before the splitting) is a direct consequence of the effect of heterogeneity on fluid focusing since the cavity extension rate is proportional to the fluid velocity.

Unlike in a homogeneous medium, there is no two-channel solution or splitting in a heterogeneous medium. Whatever the width of the initial disturbance at the inlet of the domain, only one corner of the initial rectangle produces an elongate cavity. A heterogeneous texture favors the biggest cavity among all others that are potential instabilities. Because of the strong selection process operating in the heterogeneous medium, all but a single elongated cavity are repressed even at the early stage of evolution.

In simulation H.2 (Figure 5c) there is no added initial heterogeneity near the inlet. This case can be compared to case DR.6 (Figure 1). The pattern of dissolution is qualitatively similar in both cases: At the beginning several narrow channels develop along the inlet side, then all but one stop growing, and finally, only one cavity reaches the outlet. The difference between H.2 and DR.6 is that a single cavity becomes dominant much earlier in the heterogeneous medium. As in case H.1, heterogeneity favors the biggest channel of those initiated at the inlet side, favoring one cavity much earlier than in a homogeneous medium.

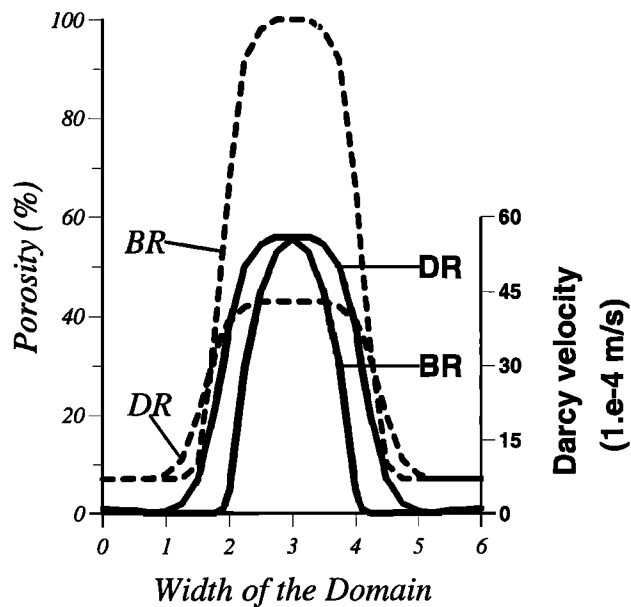


Figure 4. Porosity and Darcy velocity across a section of the domain (at 4×10^{-2} m from the inlet) through a finger (DR) and a cavity (BR). The X axis of the graph corresponds to the vertical direction of the simulation domain. Read $1.e-4$ as 1×10^{-4} .

In both cases H.1 and H.2, the dominant cavity grows straight and parallel to the largest pressure gradient. The overall length and width of the channels is the same in homogeneous and heterogeneous media. At the end of a simulation the progress of the reaction front is controlled by the overall pressure gradient and not by the local permeability as it is earlier during the simulation.

4. Summary and Discussion

The development of reaction-induced channels has been simulated numerically at experimental lengthscale and timescale, in a relatively narrow domain, in a system with large Da and Pe . This system has many characteristics of geological occurrences. Linear analysis predicts that in such a system the reaction front is unstable to the formation of channels. Our simulations include nonlinear effects and show that the width and number of these channels are determined by the characteristic of this system (expressed by Da and Pe). We performed three series of simulations to analyze the most

stable wavelength characterizing the growing channel array: (1) the Darcy regime DR, (2) the Brinkman cases BR, and (3) heterogeneous cases H. We have determined the width of the channel, by initializing the simulation with two types of conditions. The initial conditions force the active development of one single finger size that is of a size independent of the initial introduced disturbance near the inlet. On the other hand, the cases with a matrix perturbed by a white noise (all instabilities are excited) lead to the development of many channels which are soon abandoned in favor of one which grows as in the previous situation. We have shown that the elongation of the channels results from a competition between them to capture the fluid flow. Consequently, there are drastic changes in the flow pattern during the time the dissolution pattern evolves to the development of one channel rather than many. Since in each case only one channel with the same characteristic width grows to reach the outlet, regardless of the size or geometry of the initial matrix heterogeneity near the inlet, we propose that the final one-channel pattern is the global attractor of the system; that is, it is the long-time state resulting for a large class of initial data.

The influence of matrix heterogeneity on infiltration has been analyzed. It appears that the localization of hydrodynamic dispersion explains the small differences between the BR and DR cases. At the beginning of a DR simulation in a homogeneous medium, the reaction front progresses as one or two channels depending on the size of the initial heterogeneity. Even when the development of an initially wider finger is stimulated, the system never lets it develop. Instead, two smaller fingers develop, and the time during which these two fingers develop together is proportional to the distance between them. On the contrary, in BR cases the number of channels early in the simulation is independent of the initial heterogeneity size near the inlet. The same system can develop as one or two long cavities as long as numerical noise remains so low that it does not trigger any channeling. This short-lasting phenomenon is not possible in nature because of omnipresent heterogeneity of natural porous media that triggers the early development of one of the channels. The difference between the BR and DR cases is location of the dispersion at the interface between the channel and unaltered zones. In the BR case the majority of the dispersion occurs near the tip of the channel while in the DR case it is distributed more broadly everywhere inside the channel and along the interface. Finally, in the cases studied in the H series (which is the BR case with a heterogeneous

Table 1. Comparison of the Major Characteristics of DR and BR Simulations, Based on Cases DR.1 - DR.6, and BR.1 and BR.2

| | Cavities (BR) | Porous Fingers (DR) |
|------------------------------------|---|--|
| Width of single instability | $0.9 \cdot 10^{-2}$ m | $1.34 \cdot 10^{-2}$ m |
| Width Wd of multiple instability | $0.52 < Wd < 0.74 \cdot 10^{-2}$ m | $0.44 < Wd < 1.0 \cdot 10^{-2}$ m |
| Width of instability growth | constant | increasing |
| Fluid dispersion | localized in the tip | inside the finger |
| Normalized speed of reaction front | 1 | 20 |
| Two-channels instability | independent of initial heterogeneity size | heterogeneity size above which two fingers develop |

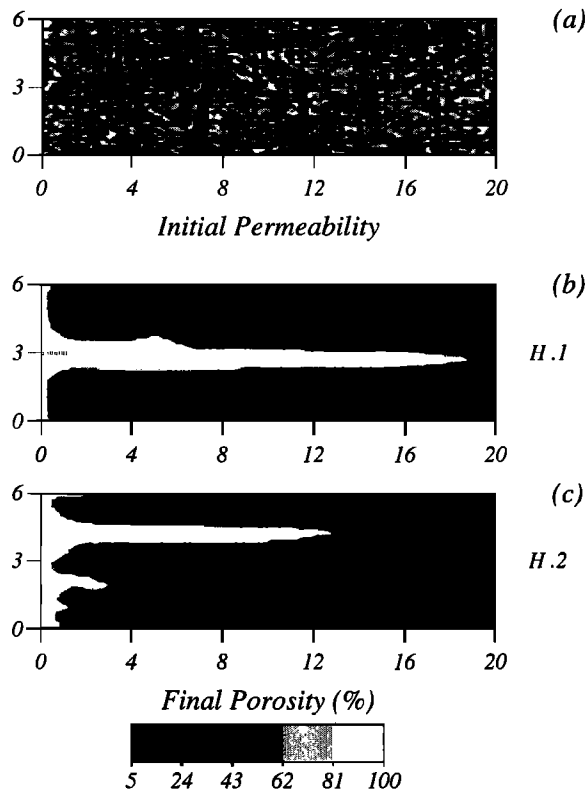


Figure 5. (a) Initial heterogeneous permeability field for the simulation of cavities in a porous medium heterogeneous everywhere (cases H.1 and H.2). There is an additional hole (size is 1.4×10^{-2} m by 0.18×10^{-2} m) in the inlet for case H.1. (b) Final porosity of simulation H.1. The initial matrix is pure calcite. The porosity is 5%. (c) Final porosity of simulation H.2

medium) the introduction of heterogeneity everywhere in the matrix gives a similar result. The instability of the reaction front strongly selects a single-channel solution, at a very early stage of the evolution. Initial heterogeneity introduced in the matrix permeability has the same effect on the reaction front instability whether it is introduced near the inlet or everywhere in the domain. When the initial matrix is heterogeneous everywhere in the domain (i.e., series H), the growth of a single cavity is favored (and is faster than in the homogeneous case) at the beginning of the simulation. When the spatial heterogeneity near the inlet is much larger than the characteristic width of a channel for the system, the reaction front again evolves into one narrow channel. Focusing favors the onset of instability, but once a channel has started growth, it is the flow pattern which controls the narrow channel growth direction. We expect that a cavity can be captured by an already existing fracture if this disturbance captures the flow associated with the channel growth. However, the cavity may develop next to the fracture when the flow is not fully captured by the feature. In a previous work, a simulation was used to show that fingering is significantly affected by a heterogeneity that extended over a spatial length of the order of L [Chen and Ortoleva, 1990]. In this paper, it is shown that when the heterogeneity includes a length scale smaller than L , the channeling grows parallel to the flow without being redirected by the matrix heterogeneity.

Concerning the time constant for the development of a finger or cavity, the progress of the reaction front itself is directly related to the magnitude of the flow. A difference between BR and DR channeling is that BR is much slower. Flow does not boost dramatically the development of a cavity because the flow velocity inside the channel is actually controlled by the permeability of the matrix lying between the tip of the channel and the outlet. If the low permeability of the porous media were not actually controlling the magnitude of the flow, we expect that the flow, and, consequently, the cavity growth, could be much faster than at the stage studied in our simulations. A consequence would be a turbulent flow due to the nonnegligible inertia in a very low viscosity fluid. This turbulence would change the dispersion of the reactive molecules in the fluid and would interact with an organized advection in the boundary layer next to the solid-fluid interface where the chemical gradients are large; this topic is beyond the scope of the present study.

In our simulations the flow pattern is controlled by a constant pressure boundary condition. This very specific flow corresponds nevertheless to the flow pattern in a limited zone of many geological situations at a given scale, which can be much larger than the sample scale. Our simulations help one to understand mechanisms involved in fluid transfer in the crust where the fluid flow induced by convection or topography brings reactive fluid (with higher solubility) in contact with the matrix. Da remains high when both G and \bar{V} are decreased by the same order of magnitude, which is the case in a geological situation because the fluid is usually much less reactive than the acid fluid of our experiments, and the large-scale Darcy flow is closer to the centimeter per year than to the kilometer per year scale. In addition, Da is proportional to L . At the scale larger than the reactive front width, our study allows an analysis of the interplay between reaction flow and initial heterogeneity in a geological system where a large-scale flow brings a reactive fluid into a rock. Channels will align with the direction of large-scale flow streamlines.

For a large-scale flow of a centimeter per year and value of a reaction coefficient for the crust, one expects reaction front width ranging between 1 μ m and 100 meters [Steefel and Lasaga, 1990]. If channels develop with a width of 100 m, they will not be noticed in core. However, the theory may help to identify them on larger-scale data like seismic profiles. In other respects our simulations show that close to the inlet of reactive fluids, many small channels can develop. A common case is that of meteoric water developing a karst network in a carbonate formation. Near the surface, numerous metric to centimetric cavities develop in a zone called "epikarst" [Mangin, 1974; Kaçaroğlu et al., 1997; Jassim et al., 1997]. We believe that this corresponds to the numerous short cavities developed at the inlet zone in our model. Water is then collected at depth to produce very few outlet pipes at the base of the karstic zone. This might result from the capture process observed in our model. At a later stage for a fully developed karst, the longest channel would modify the pressure field in such a way that it would capture the fluid from an area of a size comparable to its length. As a result, the number of the channel-like fingers or cavities in this area is related to the size of the drained area, while the channel is wider than the width of the reaction front. If this is taken into account, it is possible to estimate the density of major

channels. In an area where the large-scale flow is controlled by gravity, one can expect channels relatively parallel to each other to grow down slope. This analysis is useful to determine if the permeability structure of the sedimentary layers is dominated by a network of channels or by the matrix permeability. This has different consequences for the dispersive transport of the fluid, since the flow in a channel is orders of magnitude larger than that in a matrix with "good" permeability. These issues are central in the analysis of contaminant migration and in the context of petroleum exploration and production.

One of the most surprising implications of this study is that the long-time consequence of more complex initial data can actually lead to the acceleration of the evolution to global simplicity. Thus in the white noise case H (initial heterogeneity everywhere) the system most rapidly evolves to a state with a single cavity. There is a cascade of states from one of many small channels to that of fewer but larger channels.

Notation

| | |
|--------------|--|
| a_α | activity of species α . |
| C_α | nondimensional concentration of aqueous species. |
| C_{\max} | maximum concentration of aqueous species, $N L^{-3}$. |
| C | average concentration of aqueous species, $N L^{-3}$. |
| C_α | concentration of aqueous species α , $N L^{-3}$. |
| D | dispersion coefficient of species α in water, $L^2 T^{-1}$. |
| G_i | growth/dissolution rate of mineral i , $L T^{-1}$. |
| k_i | rate constant of mineral i reaction, $L T^{-1}$. |
| K_i | equilibrium constant of reaction for mineral i . |
| L | length scale of the width of the simulation domain, L . |
| L_r | thickness of the reaction front, L . |
| n_i | number of mineral i grains per rock volume, L^{-3} . |
| N | number of minerals. |
| P | fluid pressure, $M L^2 T^{-1}$. |
| P^* | nondimensional pressure. |
| R_i | grain radius of mineral i , L . |
| t | time. |
| t^* | non-dimensional time. |
| V | fluid velocity, $L T^{-1}$. |
| V_i | volume of the grain of mineral i , L^3 . |
| V^* | non-dimensional velocity. |
| \bar{V} | average interstitial velocity, $L T^{-1}$. |
| W^f | reaction rate of the aqueous species, $N L^{-3} T^{-1}$. |
| W^i | reaction rate of the mineral i reaction, $N L^{-3} T^{-1}$. |
| α | aqueous species. |
| χ | artificial compressibility in the numerical method. |
| ϕ | rock porosity. |
| κ | permeability of the porous medium, L^2 . |
| κ_0 | reference permeability, L^2 . |
| κ^* | nondimensional permeability. |
| μ | water viscosity, $M L^2$. |
| v_α^f | stoichiometric coefficient for species α in the aqueous reaction. |
| v_α^i | stoichiometric coefficient for species α in the mineral i reaction. |
| ρ | water mass density, $M L^{-3}$. |
| ρ_i | molar density of i mineral, $N L^{-3}$. |

Acknowledgments. We are very thankful to Pierre Genthon, with whom we had many very fruitful discussions about the geophysical issues of the model. We also thank Brigitte Bazin for the discussion which allowed us to compare successfully numerical and experimental simulations for a validation of our model. We thank the referees for their careful reviews of the manuscript. We gratefully acknowledge the National Science Foundation, Geological Sciences Program, for financial support.

References

- Adler, P., *Porous Media: Geometry and Transport*, Butterworths, London, 1992.
- Aharonov, E., J.A. Whitehead, P.B. Kelemen, and M. Spiegelman, Channeling instability of upwelling melt in the mantle, *J. Geophys. Res.*, **100**, 20,433-20,450, 1995.
- Arquis, E., Transferts en milieu poreux et à l'interface: de l'échelle microscopique à l'échelle macroscopique. Mémoire de Thèse, 208 pp., Bordeaux Univ., Bordeaux, France, 1994.
- Arquis, E., Boundary-layer flow on a perforated plate., *C. R. Acad. Sci., Ser. IIb, Mec. Phys. Chim. Astron.*, **321**, 265-272, 1995.
- Bear, J., *Dynamics of Fluids in Porous Media*, 764 pp., Elsevier Sci., New York, 1972.
- Békri, S., J.F. Thovert, and P. Adler, Dissolution of porous media, *Chem. Eng. Sci.*, **50** (17), 2765-2791, 1995.
- Bernabe, Y., Self-organized fluid-flow through heterogeneous networks, *Geophys. Res. Lett.*, **23**, 3039-3042, 1996.
- Bolton, E.W., A.C. Lasaga, and D.M. Rye, Dissolution and precipitation via forced-flux injection in a porous medium with spatially variable permeability: Kinetic control in two dimensions, *J. Geophys. Res.*, **102**, 12,159-12,171, 1997.
- Brinkman, H.C., A calculation of the viscous forces exerted by a flowing fluid or a dense swarm of particles, *Appl. Sci. Res.*, **A1**, 27-34, 1947.
- Chadam, J., D. Hoff, E. Merino, P. Ortoleva, and A. Sen, Reactive infiltration instability, *IMA J. Appl. Math.*, **36**, 207-221, 1986.
- Chadam, J., P. Ortoleva, and A. Sen, A weakly nonlinear stability analysis of the reactive infiltration interface, *SIAM J. Appl. Math.*, **48**(6), 1362-1378, 1988.
- Chen, W., and P. Ortoleva, Reaction front fingering in carbonate-cemented sandstone, *Earth Sci. Rev.*, **29**, 183-198, 1990.
- Daccord, G., Chemical dissolution of a porous medium by a reactive fluid, *Phys. Rev. Lett.*, **58**, 479-482, 1987.
- Hoefner, M.L., and H.S. Fogler, Pore evolution and channel formation during flow and reaction in porous media, *AIChE J.*, **34**, 45-54, 1988.
- Jassim S.Z., A.S. Jibril, and N.M.S. Numan, Gypsum karstification in the middle Miocene Fatha formation Mosul area, Northern Iraq, *Geomorphology*, **18**, 137-149, 1997.
- Kaçaroglu, F., M. Degirmenci, and O. Cerit, Karstification in Miocene gypsum: An example from Sivas, Turkey, *Environ. Geol.*, **30**, 88-97, 1997.
- Lichtner, P.C., The quasi-stationary approximation to coupled mass transport and fluid rock interaction in porous media, *Geochim. Cosmochim. Acta*, **52**, 143-165, 1988.
- Liu, X., A. Ormond, K. Bartko, Y. Li, and P.J. Ortoleva, Matrix acidizing analysis and design using a geochemical reaction-transport simulator, *J. Petrol. Sci. Eng.*, **17**, 181-196, 1997.
- Mangin, A., Contribution à l'étude hydrodynamique des aquifères karstiques, *Ann. Spéléol.*, **29**, 283-332, 1974.
- Ortoleva, P.J., *Geochemical Self-Organization*, Oxford Monogr. Geol. Geophys., vol. 23, Oxford Univ. Press, New York, 1994.
- Ortoleva, P.J., J. Chadam, E. Merino, and A. Sen, Geochemical self-organization II, The reactive-infiltration instability. *Am. J. Sci.*, **287**, 1008-1040, 1987.
- Ortoleva, P.J., Y. Chen, X. Liu, A. Ormond, and R. Larkin, Simulation of waste injection and migration with the fully coupled hydrologic, mineral and pore fluid reaction code CIRF.A, in *Deep Injection Disposal of Hazardous and Industrial Waste: Scientific and Engineering Aspects*, edited by J.A. Apps and Chin-Fu Tsang, pp. 627-636, Academic, San Diego, Calif., 1996.
- Peyret, R., and D.T. Taylor, *Computational Methods for Fluid Flow*, 358 pp., Springer-Verlag, New York, 1982.

- Rege, S.D., and H.S. Fogler, Competition among flow, dissolution, and precipitation in porous media, *AIChE J.*, 35, 1177-1185, 1989.
- Renard, F., J.-P. Gratier, P. Ortoleva, E. Brosse, and B. Bazin, Self-organization during reactive fluid flow in a porous medium, *Geophys. Res. Lett.*, 25, 385-388, 1998.
- Rougerie, F., C. Andrié, and P. Jean-Baptiste, Helium-3 inside atoll barrier reef interstitial water: A clue for geothermal endo-upwelling, *Geophys. Res. Lett.*, 18, 109-112, 1991.
- Schreoder, J.A., and B.A. Purser, *Reef Diagenesis*, 455 pp., Springer-Verlag, New York, 1986.
- Steeffel, C.I., and A.C. Lasaga, Evolution of dissolution patterns: Permeability change due to coupled flow and reaction, in *Chemical Modeling in Aqueous Systems II*, edited by D.C. Melchior and R.L. Basset, *Am. Chem. Soc. Symp. Ser.*, 416, 213-225, 1990.
- White, W.B., *Geomorphology and Hydrology of Karst Terrain*, 964 pp., Oxford Univ. Press, New York, 1988.
- Williams, B.B., J.L. Gidley, and R.S. Schechter, *Acidizing Fundamentals, SPE AIME Monogr.*, vol. 6, Am. Inst. of Min. and Eng., New York, 1979.
- Wolery, T. J., EQ3NR, a computer program for geochemical aqueous speciation solubility calculation: the theoretical manual, user's guide, and related documentation (version 7), *UCRL -MA-110662-PT-III* Lawrence Livermore Nat. Lab., Livermore, Calif., 1992.
-
- A. Ormond, Observatoire Midi Pyrénées / Université P. Sabatier, 14 Ave. Edouard Belin, F31401 Toulouse, France. (ormond@pontos.cst.cnes.fr)
- P. Ortoleva, Laboratory for Computational Geodynamics, Department of Chemistry, Indiana University, Bloomington, IN 47405. (ortoleva@indiana.edu)

(Received September 2, 1999; revised March 22, 2000 ;
accepted April 3, 2000.)